Journal of Power Sources 192 (2009) 43–50

Contents lists available at ScienceDirect

Journal of Power Sources

journal homepage: www.elsevier.com/locate/jpowsour

Development of anode material based on La-substituted $SrTiO_3$ perovskites doped with manganese and/or gallium for SOFC

M.J. Escudero[a,b,*], J.T.S. Irvine[b], L. Daza[a,c]

[a] Dpto Energía, CIEMAT, Av. Complutense 22, 28040 Madrid, Spain
[b] School of Chemistry, Purdie Building, University of St Andrews, St Andres, Fife KY16 9ST, UK
[c] Instituto de Catálisis y Petroleoquímica (CSIC), Campus Cantoblanco, C/Marie Curie 2, 28049 Madrid, Spain

ARTICLE INFO

Article history:
Received 15 October 2008
Received in revised form
24 November 2008
Accepted 25 November 2008
Available online 11 December 2008

Keywords:
Titanates
Perovskite
Electrical conductivity
Anode
SOFC

ABSTRACT

Materials based on La-substituted $SrTiO_3$ perovskites doped with manganese and/or gallium for SOFC have been studied as novel anodes for solid oxide fuel cell. $La_4Sr_8Ti_{11}Mn_{1-x}Ga_xO_{38-\delta}$ ($0 \le x \le 1$) oxides were synthesized by solid state reaction and the influences of the manganese and/or gallium content on the structure, morphology, thermal properties and electrical conductivity of these materials has been investigated. All compounds show cubic structure with a space group *Pm-3m*. These compounds presented high electrical conductivity values under reducing atmosphere between 7.9 and 6.8 S cm^{-1} at 900 °C. For the composition $x \ge 0.5$, the thermal expansion coefficient in both reducing and oxidizing atmosphere are close to that of SOFC electrolytes (8YSZ, CGD). In general, the substitution of Ga by Mn causes a slight reduction in each of the following, lattice parameter, degree of oxygen loss on reduction, thermal expansion coefficient, and electrical conductivity.

1. Introduction

Solid oxide fuel cells (SOFC) have grown in recognition as a viable high-temperature fuel cell technology able to convert chemical energy directly into electricity with high efficiencies unattainable from all conventional thermal engines. The high operating temperature of SOFCs (>650 °C), allows internal reforming, promotes rapid kinetics with non-precious materials and offers high flexibility in fuel choice. Various fuel options such as natural gas, methanol, ethanol and gasoline are considered feasible for SOFC operation, offering a very significant ecological dimension in the problem of effective energy conversion [1].

Currently, the most widely used anode material used in solid oxide fuel cells (SOFCs) is Ni-ytria-stabilized zirconia (YSZ) cermet. This anode displays excellent catalytic properties for fuel oxidation and good current collection but exhibits disadvantages such as easy poisoning by sulphur, carbon deposition and poor oxidation stability which cause volume instability. Nowadays, there are two main SOFC alternative anode research trends to overcome all drawbacks associated with the use of Ni-YSZ cermet [2,3]. The first is the use of alternative cermets composed of two or three single phase oxides. One phase provides catalytic properties, a second is an excellent electronic conductor and the third material can be electrolyte used in the SOFC to provide stable microstructures and to introduce ionic conductivity to extend the three phase boundary (TPB) [4]. For example, Cu-Ni-CeO_2, Cu-Co-CeO_2 [5] and Ru-Ni-GDC($Ce_{0.9}Gd_{0.1}O_{1.95}$) [6,7] exhibit substantially better performance when directly operated on hydrocarbons, as well as a high resistance to carbon deposition. The second option is to use alternative materials based on fluorite, pervoskite or tungsten bronze structures [8].

Among the perovskites, La-substituted $SrTiO_3$ materials show high electrical conductivity in reducing atmosphere, a good dimensional and chemical stability upon redox cycling, but the electrocatalytic activity for H_2 oxidation is very poor [9]. However, it is possible to improve its activity introducing dopants such as Mn and Ga in substitution on the Ti site. On the one hand, Mn is expected to adjust its valence (+4,+3,+2) according to the oxygen partial pressure, and thus it may stabilize the perovskite lattice in a way similar as in $La_{0.75}Sr_{0.25}Cr_{0.5}Mn_{0.5}O_{3-\delta}$ [10,11] (LSCM) and (La,Sr)MnO_3 (LSM) [12,13]. On the other hand, Ga is well known to adopt lower co-ordination than octahedral in perovskite-related oxides [1], and its cation has a fixed valence of +3. Then, the replacement of Ti^{4+} by a cation with lower charge would force the removal of oxygen from the structure to maintain the electroneutrality in the crystal, thus creating local oxygen vacancies that might favour ionic transport [14]. Therefore, the possibility to be a mixed ionic electronic conductor (MIEC) that could exhibit a higher catalytic activity due to the ability to transporting both ionic and electronic defects.

* Corresponding author at: Dpto Energía, CIEMAT, Av. Complutense 22, 28040 Madrid, Spain. Tel.: +34 913 466 622; fax: +34 913 466 269.
E-mail address: m.escudero@ciemat.es (M.J. Escudero).

0378-7753/$ – see front matter © 2008 Elsevier B.V. All rights reserved.
doi:10.1016/j.jpowsour.2008.11.132

Recently, a new family of pervoskite titanates with formula $La_4Sr_8Ti_{12-n}Mn_nO_{38-\delta}$ has been investigated as anode materials for SOFC, with $n = 1$ being more suitable [15]. Ruiz Morales et al. [1,16] have reported an excellent fuel cell performance on wet hydrogen and methane using $La_4Sr_8Ti_{11}Mn_{0.5}Ga_{0.5}O_{38-\delta}$ anode. On the basis of these investigations, the system $La_4Sr_8Ti_{11}Mn_{1-x}Ga_xO_{38-\delta}$ ($0 \le x \le 1$) has been studied as potential anode materials. In this work, $La_4Sr_8Ti_{11}Mn_{1-x}Ga_xO_{38-\delta}$ ($0 \le x \le 1$) perovskites have been synthesized with differing gallium contents and their influence on the structure, morphology, thermal properties, and electrical conductivity has been evaluated.

2. Experimental

$La_4Sr_8Ti_{11}Mn_{1-x}Ga_xO_{38-\delta}$ ($x = 0$, 0.25, 0.50, 0.75, 1) oxides were synthesized by solid state reaction. Stoichiometric amounts of predried high purity La_2O_3 (Alfa Aesar, 99.99%), $SrCO_3$ (Aldrich, 99.9%), TiO_2 (Aldrich, 99.9%), Mn_2O_3 (Aldrich 99%) and Ga_2O_3 (Alfa Aesar, 99.999%) were mixed in acetone and then calcined at 1000 °C for 6 h. The resulting powders were subsequently ground in acetone in zirconia ballmills for 4 h, and uniaxially pressed into pellets and finally fired in air at 1400 °C for 50 h. Reduced phases were obtained by further reduction at 1000 °C under flowing 5% H_2/Ar for 72 h.

The phase composition of raw and reduced powders was determined by X-ray powder diffraction (XRD) using a Stoe StadiP Transmmission X-ray diffractometter equipped with Cu $K\alpha_1$ radiation ($\lambda = 1.5406$ Å). The diffraction patterns were recorded in the 2θ range 20–85° in steps of 0.1° at 90 s/step. Rietvelt refinements of the crystal structure were performed using the FULLPROF program (Windows version, September 2007) in order to calculate the lattice parameters. The line shape of the diffraction peaks was generated by a pseudo-Voigt profile function.

The Mn oxidation state was evaluated by X-ray absorption near-edge structure (XANES) measurements performed at the European Radiation Synchrotron Facility (ESRF, France) on beamline BM25A. Mn K-edge absorption spectra were measured for the samples $La_4Sr_8Ti_{11}Mn_{1-x}Ga_xO_{38-\delta}$ ($x = 0$, 0.75) before and after reduction at room temperature using the monochromator in fluorescence detection mode. The solid samples were mounted on the sample holder using carbon tape.

The morphology of the samples was characterized before and after the reduction by scanning electron microscopy (SEM) using a JEOL JSM-5600 microscope.

Thermogravimetric analyses (TGA) were carried out in order to determine the oxygen stoichiometry changes of the samples. The TGA experiments were conducted on a Rheometric Scientific TG1000 M instrument. Pre-reduced samples were heated in a flowing air atmosphere (35 ml min^{-1}), at a ramp rate of 5 °C min^{-1} to 850 °C, held for 6 h and then cooled at 5 °C min^{-1}. The increase of weight during the oxidation was used to calculate the oxygen content change (δ).

Dense compounds are required for the measurements of thermal expansion coefficient and electrical conductivity. The prepared powders were pressed into pellets (12 mm in diameter and 3.5 mm think) using 3 tons of uniaxial pressure during 30 s. The thermal expansion coefficient of dense ceramics was studied in a NETZSCH DIL 402 C (alumina holder) with a TSAC 414/4 controller. The samples were tested in 5% H_2/Ar (50 ml min^{-1}) in the temperature range of room temperature to 850 °C with a ramp rate of 4 °C min^{-1} and then cooled in air (50 ml min^{-1}).

The electrical conductivity of the samples was measured by the DC four-probe method using a Keithley 220 current source and a Schlumberger Solartron 7150 digital multimeter. Firstly, the measurements were carried out as a function of temperature in dry 5%H_2/Ar with a ramp rate of 1 °C min^{-1}. Secondly, the temperature was held constant at 900 °C for 24 h to try to ensure a total reduction. Then, they were cooled to 50 °C and heated 900 °C in reducing conditions with a ramp rate of 1 °C min^{-1}. High-temperature conductivity measurements as a function oxygen partial pressures, $p(O_2)$, from 10^{-20} atm to air were performed at 900 °C. The $p(O_2)$ values were monitored using a YSZ oxygen sensor placed next to the pellet in the cell. Finally, the measurements of conductivity were carried out in air as function of temperature.

3. Results and discussion

3.1. Structural characterization

Pervoskite oxides, $La_4Sr_{n-4}Ti_nO_{3n+2}$, are often reported in the literature as simple cubic phase, whose main feature is their ability to accommodate extra oxygen beyond the parental ABO_3 perovskite. The structure of these compounds can be described as layered phases, having oxygen-rich phases in the form of crystallographic shears joining consecutive perovskite blocks. These planes become more sporadic with increasing n (lower oxygen content) until the layered structure is lost for $n > 11$ [17]. In this structure, the excess oxygen is randomly distributed within the perovskite framework. The presence of extra oxygen could affect both the structure and the electrochemical properties.

As determined from XRD, all samples after sintering in air at 1400 °C for 50 h showed a single phase perovskite-type structure (Fig. 1a). After reduction in 5% H_2/Ar at 1000 °C for 72 h, all compositions retained the perovskite structure (Fig. 1b). Before and after reduction, the structure of all compounds at room temperature is cubic with a space group *Pm-3m*. The calculated lattice parameters of the system $La_4Sr_8Ti_{11}Mn_{1-x}Ga_xO_{38-\delta}$ ($x = 0$, 0.25, 0.50, 0.75 and 1) in the oxidized and reduced state are shown in Table 1, while the lattice parameters are displayed in Fig. 2

In oxidizing atmosphere, the incorporation of Ga instead of Mn in the lattice decreases cell edge linearly except for the composition $x = 0.5$. This decrease could be due to the lower ionic radius and lesser degree of distortion of Ga^{3+} (0.620 Å) [18] than that of Mn^{3+} (0.645 Å), as well as perhaps some changes in the oxygen non-stoichiometry on the incorporation of gallium in the structure. The composition with $x = 0.5$, which has the same amount of manganese and gallium, could be a critical value that determines defect are ordering in the structure.

In reducing atmosphere, both Mn and Ti tend to have lower valence and larger ionic radii, giving larger lattice parameters. The reduction of these cations causes the removal of oxygen from the structure, creating oxygen vacancies to maintain the electroneutrality. Therefore, all samples show an increase of volume being more important for the samples with higher Mn content, hence decrease in Mn ionic size on reduction is the most important factor. Additionally reduction of Ti^{4+} to Ti^{3+} may contribute producing a lattice expansion due to the Ti^{3+} radius (0.67 Å) being higher than that of Ti^{4+} (0.650 Å). The substitution of Ga^{3+} by Mn^{3+} (0.65 Å) and/or

Table 1
Calculated unit cell parameters from XRD of the system $La_4Sr_8Ti_{11}Mn_{1-x}Ga_xO_{38-\delta}$ ($x = 0$, 0.25, 0.50, 0.75 and 1) in the oxidized and reduced states. The numbers in brackets indicate the error in the last significant figure.

Composition	Oxidized		Reduced	
X	a (Å)	V (Å^3)	a (Å)	V (Å^3)
0	3.9196(1)	60.219(4)	3.9293(3)	60.667(9)
0.25	3.9177(2)	60.131(5)	3.9283(3)	60.621(9)
0.50	3.9123(2)	59.883(6)	3.9224(3)	60.349(8)
0.75	3.9132(2)	59.925(4)	3.9215(3)	60.306(7)
1.0	3.9119(2)	59.865(5)	3.9138(3)	59.952(7)

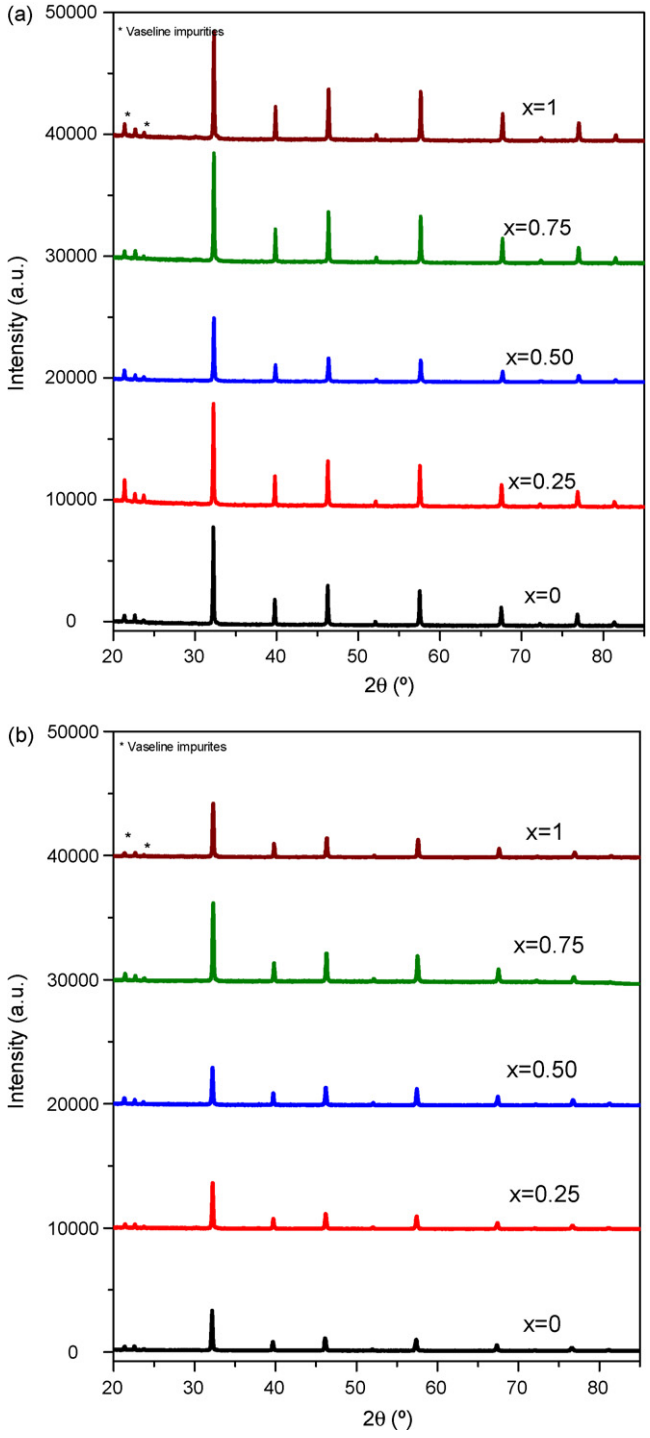

Fig. 1. XRD patterns of $La_4Sr_8Ti_{11}Mn_{1-x}Ga_xO_{38-\delta}$ (x = 0, 0.25, 0.50, 0.75, 1) oxides: (a) in oxidized state; (b) reduced state.

part of Mn^{2+} (0.820 Å) also produced a reduction of lattice parameter due the lower ionic radius of Ga^{3+}. This is in agreement with the expected reduction of manganese, so the ionic radius of this element increases to diminish its oxidation state.

XANES spectra of the Mn edge of the samples $La_4Sr_8Ti_{11}Mn_{1-x}Ga_xO_{38-\delta}$ (x = 0, 0.50, 0.75) before and after reduction at room temperature, as well as $La_{0.8}Sr_{0.2}MnO_3$ (LSM, Praxair) are illustrated in Fig. 3. All spectra are very similar to each other showing the same general shape as the perovskite oxide as $La_{0.8}Sr_{0.2}MnO_3$ (LSM). The main differences among spectra

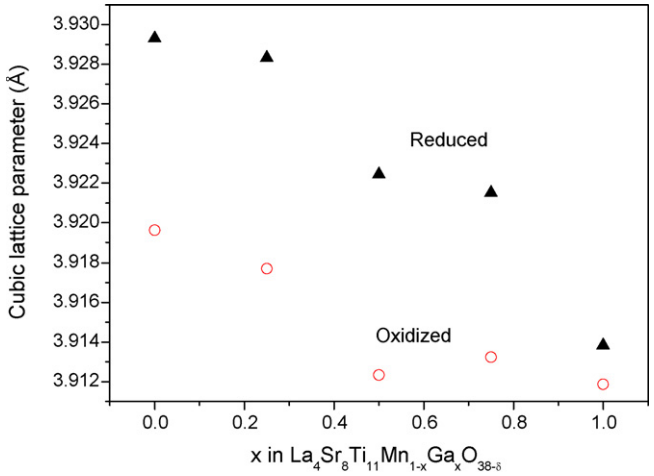

Fig. 2. Cubic lattice parameters of $La_4Sr_8Ti_{11}Mn_{1-x}Ga_xO_{38-\delta}$ (x = 0, 0.25, 0.50, 0.75, 1) oxides in both oxidized and reduced states.

are related to the chemical shift of the main peak towards lower energies for the reduced samples, and that, the Mn K edges are wider in oxidized samples.

The threshold energies (E_0) are obtained from the inflection point of the edge and presented in Table 2. As can be seen, in oxidized atmosphere, the Mn K threshold energy increases 1.2 eV in the sample with a Ga content of 0.75 indicating an increase of Mn^{4+} proportion. After the reduction, a chemical shift of 1.3 and 2.7 eV

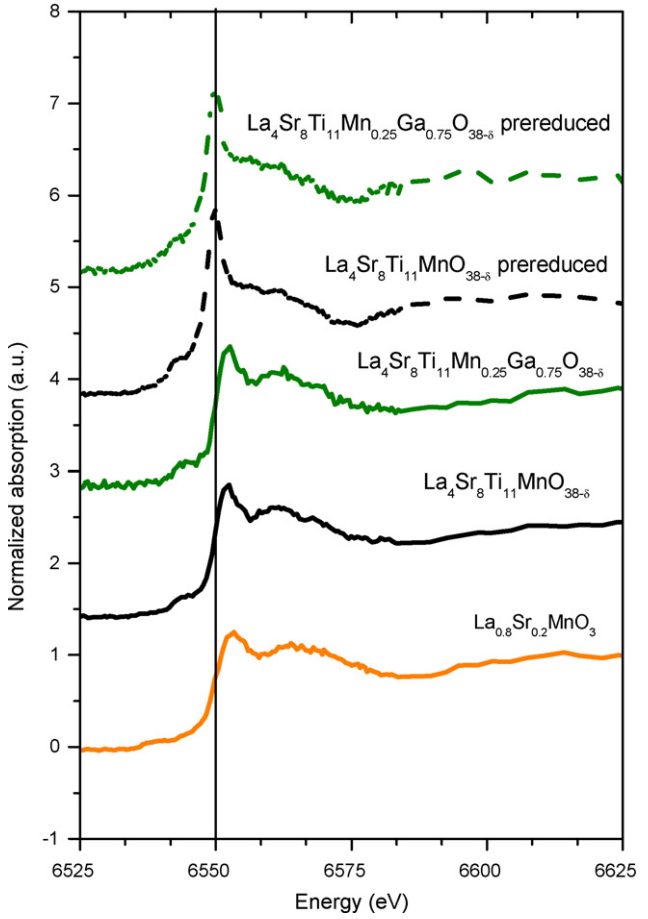

Fig. 3. The normalized Mn K-edge XANES spectra at room temperature for $La_4Sr_8Ti_{11}Mn_{1-x}Ga_xO_{38-\delta}$ (x = 0, 0.75) oxidized and reduced states and $La_{0.8}Sr_{0.2}MnO_3$.

Table 2
Threshold energies (E_0) of Mn K-edge for $La_4Sr_8Ti_{11}MnO_{38-\delta}$ and $La_4Sr_8Ti_{11}Mn_{0.25}Ga_{0.75}O_{38-\delta}$ in the oxidized and reduced states, and $La_{0.8}Sr_{0.2}MnO_3$ and estimated Mn oxidation state.

Compound	E_0 (eV)		Mean Mn oxidation state	
	Oxidized	Reduced	Oxidized	Reduced
$La_4Sr_8Ti_{11}MnO_{38-\delta}$	6549.8	6548.5	+3.1	+2.8
$La_4Sr_8Ti_{11}Mn_{0.25}Ga_{0.75}O_{38-\delta}$	6551.0	6548.3	+3.3	+2.8
$La_{0.8}Sr_{0.2}MnO_3$	6551.0		+3.3	

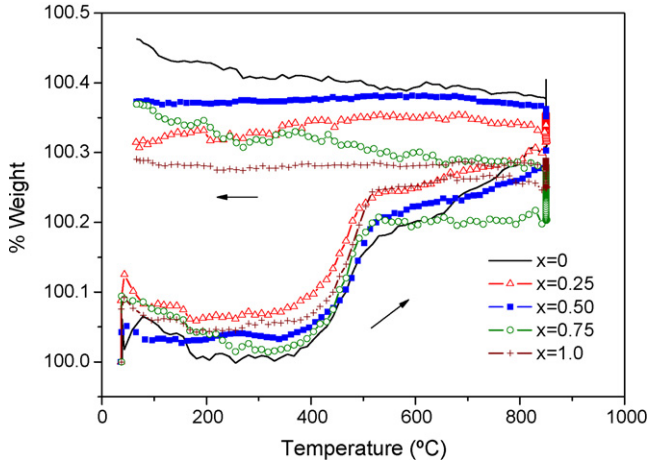

Fig. 4. TG experiments recorded during the oxidation of pre-reduced samples of $La_4Sr_8Ti_{11}Mn_{1-x}Ga_xO_{38-\delta}$ ($x = 0$, 0.25, 0.50, 0.75, 1) in air.

is observed for the samples with $x = 0$ and 0.75, respectively, with very close E_0 values. This shift could be related to with a reduction in the oxygen coordination and oxidation state. Furthermore, greater peak broadening can be observed in the oxidized samples than in the reduced ones. This could mean slight changes in the local structure around the Mn atom. In order to evaluate the oxidation state of Mn in each compound, the data of threshold energies for pure Mn, MnO, Mn_2O_3, MnO_2, $LaMnO_3$ and $CaMnO_3$ collected by Subía et al. [19] have been used. Mean Mn oxidation states have been estimated from a lineal fitting procedure and are given in Table 2. The existence of Mn^{3+} and Mn^{4+} (lower part) in the oxidized samples and the presence of Mn^{3+} and Mn^{2+} (lower part) in the reduced samples can be deduced.

3.2. Thermal analysis

The oxygen content of all reduced samples was investigated by thermogravimetric analysis (TGA). Previously, all compounds were reduced in 5%H_2/Ar at 1000 °C during 72 h. Fig. 4 shows the TGA analyses of the prereduced samples in air. From the % of weight regained for each prereduced compound, its change in oxygen non-stochiometry has been estimated and is given in Table 3. The change of oxygen atoms per unit cell is between 0.05 and 0.03 and the amount of oxygen regained becomes slightly smaller on increasing gallium content which could be due to the replacement of Ga^{3+} by

Table 3
TGA data of the system $La_4Sr_8Ti_{11}Mn_{1-x}Ga_xO_{38-\delta}$ ($x = 0$, 0.25, 0.50, 0.75 and 1). $\Delta\delta$ is the amount of oxygen atoms loss per formula unit.

Composition X	(%) wt. gain on reoxidation	$\Delta\delta$
0	0.43	−0.05
0.25	0.37	−0.05
0.50	0.33	−0.04
0.75	0.31	−0.04
1.0	0.24	−0.03

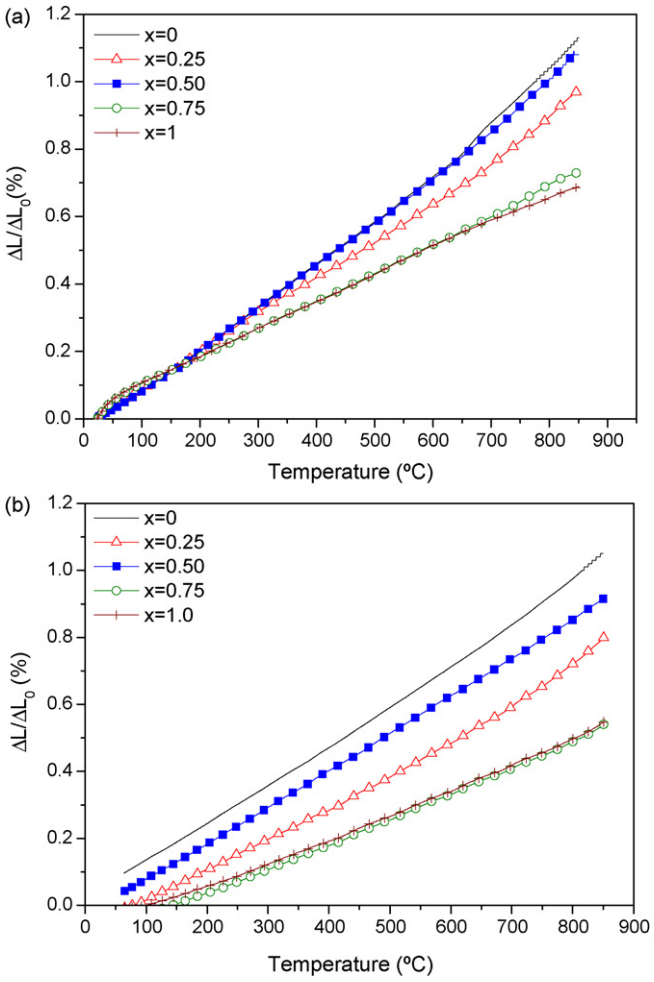

Fig. 5. Lineal thermal expansion $\Delta L/L_0$ for the samples $La_4Sr_8Ti_{11}Mn_{1-x}Ga_xO_{38-\delta}$ ($x = 0$, 0.25, 0.50, 0.75, 1): (a) in 5%H_2/Ar; (b) in air.

Mn^{4+} or Ti^{4+}, which would remove some oxygen of the structure to maintain the electroneutrality.

The thermal expansion of the samples $La_4Sr_8Ti_{11}Mn_{1-x}Ga_xO_{38-\delta}$ ($x = 0$, 0.25, 0.50, 0.75, 1) in 5% H_2/Ar, and air is shown in

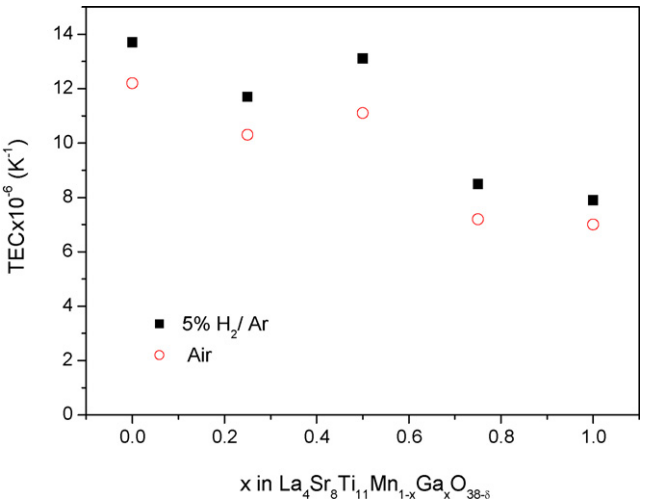

Fig. 6. Evolution of the thermal expansion coefficient (TEC) for the system $La_4Sr_8Ti_{11}Mn_{1-x}Ga_xO_{38-\delta}$, $x = 0$, 0.25, 0.50, 0.75, and 1 as a function of gallium content calculated from dilatometric data in 5%H_2/Ar and air in the temperature range at 850–50 °C.

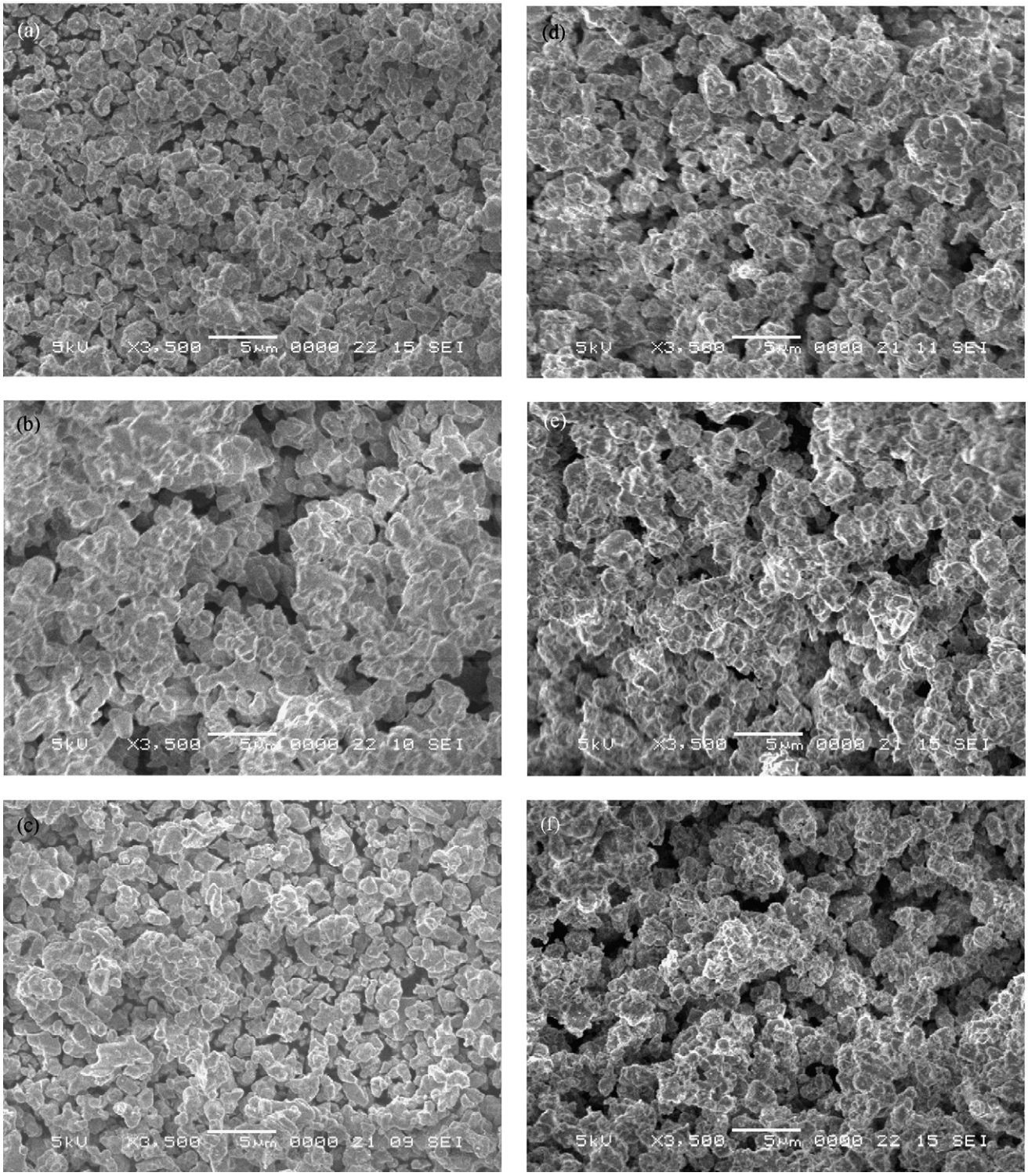

Fig. 7. SEM micrographs: (a) $La_4Sr_8Ti_{11}MnO_{38-\delta}$ in air; (b) $La_4Sr_8Ti_{11}Mn_{0.5}Ga_{0.5}O_{38-\delta}$ in air; (c) $La_4Sr_8Ti_{11}GaO_{38-\delta}$ in air; (d) $La_4Sr_8Ti_{11}MnO_{38-\delta}$ in 5% H_2/Ar; (e) $La_4Sr_8Ti_{11}Mn_{0.5}Ga_{0.5}O_{38-\delta}$ in 5% H_2/Ar; (f) $La_4Sr_8Ti_{11}GaO_{38-\delta}$ in 5% H_2/Ar.

Fig. 5. The average thermal expansion coefficients (TEC) obtained from the slope of the line in the temperature range 50–850 °C as a function of Ga content is illustrated in Fig. 6. The TEC values are between 13.7 and $7.9 \times 10^{-6}\,K^{-1}$ under reducing atmosphere and between 12.7 and $7.0 \times 10^{-6}\,K^{-1}$ under oxidizing atmosphere and, in general, all values tend to decrease with the introduction of Ga, except for the sample with $x = 0.5$, which is close to the free Ga sample. These results are in agreement with the lattice parameters calculated from XRD data. Under reducing atmosphere, the lattice expansion is a consequence of higher ionic radius and oxygen vacancies. Moreover, the increase in Ga content reduces the uptake of oxygen on reoxidation. As before mentioned, the compound with $x = 0.5$ could have some reorganization of structural defects. The thermal expansion coefficients for the samples with

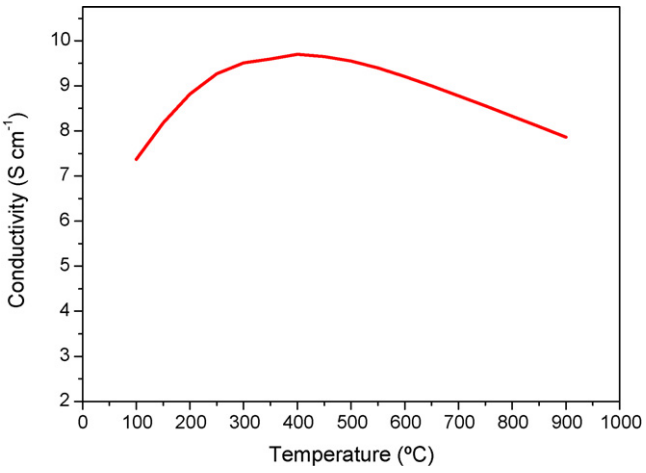

Fig. 8. Electrical conductivity of $La_4Sr_8Ti_{11}Mn_{0.75}Ga_{0.25}O_{38-\delta}$ under 5%H_2/Ar in the temperature range at 100–900 °C.

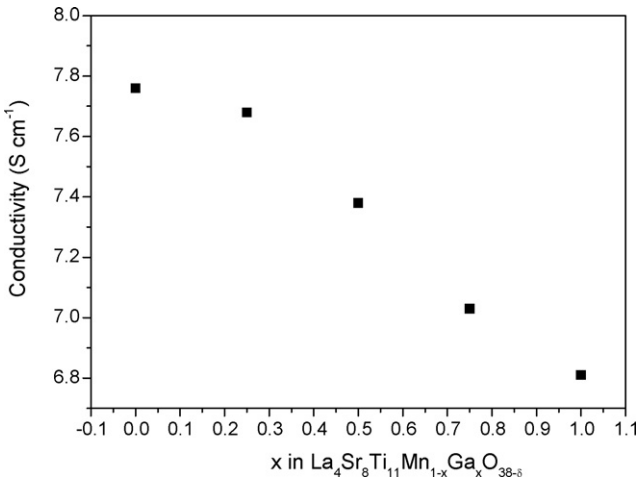

Fig. 9. Evolution of the electrical conductivity for the system $La_4Sr_8Ti_{11}Mn_{1-x}Ga_xO_{38-\delta}$, $x = 0$, 0.25, 0.50, 0.75, 1, in 5%H_2/Ar at 900 °C.

$x \geq 0.5$ are close to that of 8YSZ (10.7×10^{-6} K^{-1}) and $Ce_{0.9}Gd_{0.1}O_{1.95}$ (13.2×10^{-6} K^{-1}) [20], the electrolytes usually utilized in SOFC.

3.3. Morphology analyses

The morphology of the samples in pellet was studied by SEM before and after their reduction in 5% H_2/Ar at 1000 °C during 72 h. All compositions presented a good pore distribution and a particle size around 4 μm. As can be seen from Fig. 7, only, slight changes were observed on changing the degree of substitution of Ga by Mn or by the reduction, except for $La_4Sr_8Ti_{11}GaO_{38-\delta}$, which shows less agglomeration of particles, after reduction (Fig. 7f).

3.4. Electrical conductivity

The electrical conductivities of the $La_4Sr_8Ti_{11}Mn_{1-x}Ga_xO_{38-\delta}$ ($x = 0$; 0.25, 0.50, 0.75 and 1) in 5% H_2, air, and as function of oxygen pressure at 900 °C were measured by the DC four-terminal method.

In reducing atmosphere, all samples studied show a transition of semiconductor to metallic below ~400 °C. As an example, Fig. 8 illustrates the total conductivity of $La_4Sr_8Ti_{11}Mn_{0.75}Ga_{0.25}O_{38-\delta}$ in 5% H_2 in the temperature range of 100–900 °C. A change in the conduction regime can be observed from semiconducting-like below 400 °C, exhibiting a maximum conductivity of 9.7 S cm^{-1}, followed by a metallic behaviour at high-temperature, characterized by a negative slope. Canales-Vázquez et al. [21] observed similar behaviour in $La_2Sr_4Ti_6O_{19-\delta}$ and mentioned that this transition could be two different origins. The first is that the distribution of Ti^{3+} changes. At temperatures below 400 °C, Ti^{3+} is distributed forming long distance couples (Ti^{3+}-O-Ti^{3+}) that disappear at higher temperatures leading to Ti^{3+} randomly distributed in the structure. These ordered couples would have a partial localisation of electrons avoiding in this way the formation of a metallic band due to the presence of some discrete levels of energy. While at temperature above 400 °C, the Ti^{3+} are not in couples anymore, forming the metallic band. The second alternative suggests the two components (metallic and semiconductor) could be both in the bulk or it could be a semiconducting grain boundary and a metallic grain. The overall conductivity measured at 900 °C in 5% H_2 as a function of Ga content is shown in Fig. 9. As can be seen, the conductivity values measured were between 7.9 and 6.8 S cm^{-1}, showing a decrease of the electrical conductivity as the content of Ga increases. These high values of the electrical conductivity are due to Ti^{3+} having a positive effect on the electrical conductivity. So in reducing conditions, the interstitial oxygen is removed from the lattice creating oxygen an excess of electrons eĭ (n-type conductors). Moreover, the substitution of Mn by Ga slight decreases the non-stochiometry oxygen content (as shown TG data). This could be explain the slight reduction of the conductivity with increasing of Ga content.

The Arrhenius plots obtained in air revealed that the electrical conductivity of the samples decreases dramatically around three or four orders of magnitude compared to reduced samples and increases with the temperature what corresponding to a semiconductor behaviour, as can be seen in Fig. 10 for $La_4Sr_8Ti_{11}Mn_{0.75}Ga_{0.25}O_{38-\delta}$. This composition presents an activation energy of 0.49 eV and an electrical conductivity of 0.0065 S cm^{-1} at 900 °C. This value is three orders lower than in reducing atmosphere. It is due that the oxidized samples not containing Ti^{3+}. The replacement of Ga by Mn, causes a slight reduction of conductivity values with Ga content, for the compounds $La_4Sr_8Ti_{11}Mn_{1-x}Ga_xO_{38-\delta}$ ($x = 0$, 0.25, 0.75 and 1) at 900 °C as can be seen in Fig. 11.

The electrical conductivity of the system $La_4Sr_8Ti_{11}Mn_{1-x}Ga_xO_{38-\delta}$ ($x = 0.25$, 0.75 and 1) was measured as a function of oxygen partial pressure ($p(O_2)$) at 900 °C. The log conductivity decreases with decreasing $\log p(O_2)$, so all compounds show typical n-type conductivity as the dominant electronic mechanism. Between oxygen partial pressure of 10^{-20} and 10^{-14} atm, conductivity shows $p(O_2)^{-1/5}$ dependence for the

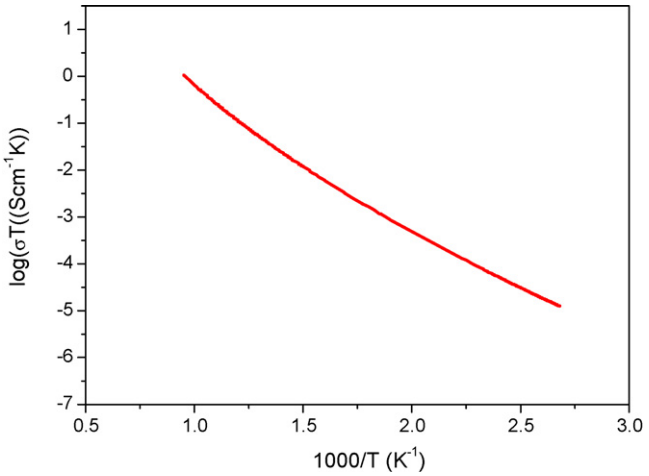

Fig. 10. Arrhenius plot of the electrical conductivity of $La_4Sr_8Ti_{11}Mn_{0.75}Ga_{0.25}O_{38-\delta}$ in air.

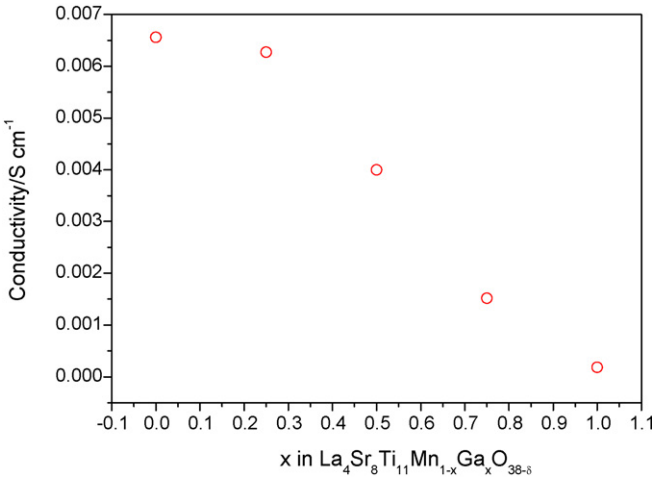

Fig. 11. Evolution of the electrical conductivity for the system $La_4Sr_8Ti_{11}Mn_{1-x}Ga_xO_{38-\delta}$, $x = 0$, 0.25, 0, 50, 0.75, 1, in air at 900 °C.

samples with $x = 0.25$ and $x = 0.75$, and $p(O_2)^{-1/4}$ for $x = 1$, free Mn sample. As an example, Fig. 12 displays the total conductivity of $La_4Sr_8Ti_{11}Mn_{0.75}Ga_{0.25}O_{38-\delta}$ as a function of pO_2 at 900 °C.

The n-type conduction of these compounds could be explained by reduction of Ti^{4+} to Ti^{3+}, the removal of oxygen from the structure creates oxygen vacancies:

$$2[Ti_{Ti}^{x}] + [O_O^x] \Leftrightarrow 2[Ti_{Ti}^{'}] + V_O^{\bullet\bullet} + \frac{1}{2}O_2(g) \quad (1)$$

At low pO_2 range, region from 10^{-19} to 10^{-14} atm, the reduction increases the oxygen deficiency. When reduction of an oxide is accommodated by the formation of $[V_O^{\bullet\bullet}]$, the electron concentration follows the relation $n \propto p(O_2)^{-1/6}$. On the other hand, if the concentration of oxygen vacancies can be fixed by chemical doping, and the conductivity is proportional to the concentration of electrons, the slope dependence is −1/4.

Therefore, the $p(O_2)^{-1/5}$ dependence could be due to the defects being titanium interstitials instead of oxygen vacancies as suggested Chiang et al. [22] for TiO_2. Thus, the Mn could promote the presence of titanium interstitials. However, these authors pointed out also that difference in slope may be slight compared to the precision of experimental data (i.e., 1/6 vs. 1/5 or 1/5 vs.1/4 slopes). So, the pO_2 dependence could not discriminate between oxygen vacancies or titanium interstitials mechanisms, for a definitive interpretation.

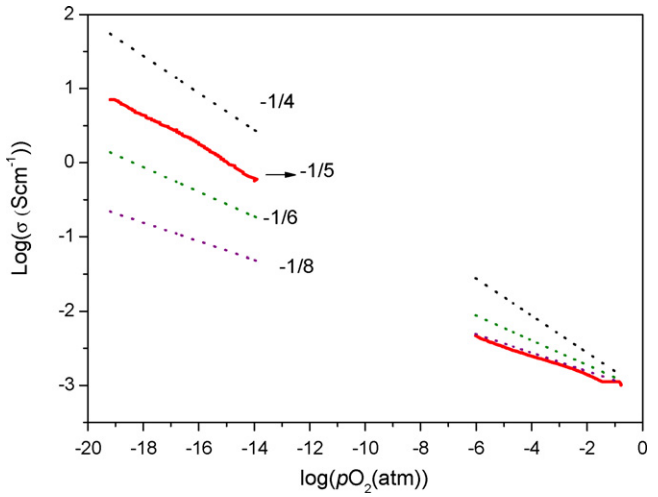

Fig. 12. Electrical conductivity for the $La_4Sr_8Ti_{11}Mn_{0.25}Ga_{0.75}O_{38-\delta}$ oxides (open circles), as function of oxygen partial pressure at 900 °C.

In the high pO_2 range, region from 10^{-6} to 10^{-2} atm, very little Ti^{3+} is likely to exist in the material; however, the behaviour is n-type so Ti^{3+} must still dominate behaviour. Due to excess oxygen in this system $La_4Sr_8Ti_{11}Mn_{1-x}Ga_xO_{38-\delta}$, oxygen vacancies are unlikely to exit. The small concentration of both electronic charge carrier $[Ti_{Ti}^{'}]$ and ionic charge carrier $[O_O^x]$ results in very low electrical conductivity with a low dependency of oxygen pressure (−1/8).

4. Conclusions

Perovskites of $La_4Sr_8Ti_{11}Mn_{1-x}Ga_xO_{38-\delta}$ $(0 \le x \le 1)$ have been studied to investigate the suitabilities of their properties for possible use as novel anode materials for solid oxide fuel cells.

All compounds have a single phase in space group *Pm-3m* that is stable in oxidizing and reducing atmospheres. It was estimated that a mean Mn oxidation state of 3.3 exists in air and 2.8 after reduction. Therefore, these data reveal the presence in the structure of net Mn^{4+} and Mn^{3+} in air and Mn^{3+} and Mn^{2+} in reducing conditions.

The concentration of excess oxygen atoms per unit cell was between 0.05 and 0.03, slight decreasing with increasing of gallium content. The thermal expansion coefficient values measured were between 13.7 and $7.9 \times 10^{-6}\,K^{-1}$ in 5% H_2 and between 12.7 and $7 \times 10^{-6}\,K^{-1}$ in air at 850 °C. The TEC for the samples with $x \ge 0.5$ are close to that of 8YSZ and $Ce_{0.9}Gd_{0.1}O_{1.95}$ electrolytes usually utilized in SOFC.

In reducing conditions, all compositions showed high electrical conductivity values in the range of 7.9–6.8 S cm^{-1} at 900 °C, revealing a transition from semiconductor to metallic below 400 °C. In air, semiconductor behaviour was observed, as well as an important decrease of electrical conductivity of about three and four magnitude orders. The electrical conductivity decreases with increasing the oxygen partial pressure values, showing the typical behaviour of an n-type conductor.

In general, the substitution of Ga by Mn causes a slight reduction in the lattice parameter, ease of oxygen removal, thermal expansion coefficient, and electrical conductivity.

These materials showed promising properties for use as anode materials for SOFC, according to the thermal analysis could be more interesting the composition with a Mn content ≥ 0.5. However, further works are required in order to evaluate the polarization resistance in operation conditions.

Acknowledgements

This work is performed in the framework of ENERCAM-CM program (Ref. S-0505/ENE-304) from Comunidad de Madrid. MJE is also grateful to the Spanish Innovation and Science Ministry for financial support by means of the "Estancias de profesores de investigadores españoles (PR2007-0214)" and JTSI group (University of St Andrews) for help in the use of facilities.

References

[1] S.L. Douvartzidesa, F.A. Coutelierisa, A.K. Deminb, P.E. Tsiakarasa, International Journal of Hydrogen Energy 29 (2004) 375–379.
[2] Y. Matsuzaki, I. Yasuda, Solid State Ionics 132 (2000) 261–269.
[3] B.C.H. Steele, I. Kelly, H. Middleton, R. Rudkin, Solid State Ionics 28 (1988) 1547–1552.
[4] J.C. Ruiz-Morales, J. Canales-Vázquez, C. Savaniu, D. Marrero-López, P. Nuñez, W. Zhou, J.T.S. Irvine, Phys. Chem. Chem. Phys. 9 (2007) 1821–1830.
[5] S.-I. Lee, J.M. Vohs, R.J. Gore, J. Electrochem. Soc. 151 (9) (2004) A1319–A1323.
[6] T. Hibino, A. Hashimoto, K. Asano, M. Yano, M. Suzuki, M. Sano, Electrochem. Solid. State Lett. 5 (2002) A242–A244.
[7] T. Hibino, A. Hashimoto, K. Asano, M. Yano, M. Suzuki, M. Sano, Electrochim. Acta 48 (2003) 2531–2537.
[8] C. Sun, S. Stimming, J. Power Sources 171 (2007) 247–260.
[9] O.A. Marina, N.L. Canfield, J.W. Stevenson, Solid State Ionics 149 (2002) 21–28.

[10] S.W. Tao, J.T.S. Irvine, Nat. Mater. 2 (2003) 320–323.
[11] S.W. Tao, J.T.S. Irvine, J. Electrochem. Soc. 153 (4) (2006), D/4-D83.
[12] I. Yasuda, M. Hishinuma, J. Solid State Chem. 123 (1996) 382–390.
[13] J. Mizusaki, Y. Yonemura, H. Kamata, K. Ohyama, N. Mori, H. Takai, H. Tagawa, M. Dokiya, K. Naraya, T. Sasamoto, H. Inaba, T. Hashimoto, Solid State Ionics 132 (2000) 167–180.
[14] C. Navas, H.L. Tuller, H.-C. zur Loye, J. Eur. Ceram. Soc. 19 (1999) 737–740.
[15] A. Ovalle, J.C. Ruiz-Morales, J. Canales-Vázquez, C. Savaniu, D. Marrero-López, J.T.S. Irvine, Solid State Ionics 177 (2006) 1997–2003.
[16] J.C. Ruiz-Morales, J. Canales-Vázquez, C. Savaniu, D. Marrero-López, P. Nuñez, W. Zhou, J.T.S. Irvine, Nature 439 (2006) 568–571.
[17] J. Canales-Vázquez, M.J. Smith, J.T.S. Irvine, W. Zhou, Adv. Funct. Mater. 15 (2005) 1000–1008.
[18] R.D. Shannon, Acta Cryst. A32 (1976) 751–767.
[19] G. Subías, J. Garcia, M.G. Proietti, J. Blasco, Phys. Rev. B 56 (1997) 8183–8191.
[20] X.D. Zhou, B. Scarfino, H.U. Anderson, Solid State Ionics 175 (2004) 19–22.
[21] J. Canales-Vázquez, S.W. Tao, J.T.S. Irvine, Solid State Ionics 159 (2003) 159–165.
[22] Y.M. Chiang, D.P. Birnie, W.D. Kingery, Physical Ceramics: Principles for Ceramic Science and Engineering, John Wiley & Sons, Inc., 1996, pp. 142–147.